CHEMISTRY OF MATERIALS

ARTICLE

pubs.acs.org/cm

Covalent Grafting to μ-Hydroxy-Capped Surfaces? A Kaolinite Case Study

Dunja Hirsemann,[†] Thomas K.-J Köster,[‡] Julia Wack,[†] Leo van Wüllen,[‡] Josef Breu,*[,†] and Jürgen Senker*[,†]

[†]Lehrstuhl für Anorganische Chemie I, Universität Bayreuth, D-95440 Bayreuth, Germany

[‡]Institut für Physikalische Chemie, WWU Münster, D-48149 Münster, Germany

Supporting Information

ABSTRACT: All μ-hydroxyl groups are frequently encountered capping groups found on the external surfaces of various minerals that are often used as fillers in composite materials. Covalent grafting to this functional group would therefore offer a versatile and attractive route to surface modification. The octahedral layer of kaolinite is composed of μ-bridged aluminol groups. In particular, intercalation compounds of kaolinite, where all basal planes are exposed and may be modified, are ideally suited to study the feasibility of such covalent graftings. The huge (internal) specific surface area greatly improves the sensitivity of the analytics and renders kaolinite an ideal model compound. Herein we analyze the mode of bonding of ethylene glycol (EG), intercalated into kaolinite (EG kaolinite), by solid-state NMR techniques. ^{27}Al MQMAS allows for distinction between intercalated and grafted EG molecules because the chemical surroundings of octahedrally coordinated aluminum nuclei in the layer are significantly changed by the formation of a covalent bond. Moreover, the temperature-dependent dynamics of the EG molecules in the interlamellar space are examined by wide-line solid-state ^{1}H NMR measurements. The EG molecules perform a circular motion around the covalently bonded hydroxyl group in the interlamellar space. Analysis of the ^{13}C−^{27}Al REAPDOR measurement in conjunction with the EG dynamics allows for determination of the ^{13}C···^{27}Al distance between octahedral aluminum and the bonded carbon atom of EG. This distance is 3.1 Å. A thorough description of the bonding mode of the EG molecules is provided and proves beyond any doubt the covalent grafting. This suggests that the reactivity of μ-hydroxyl groups, in general, is sufficient to realize a covalent surface modification of a wide range of minerals.

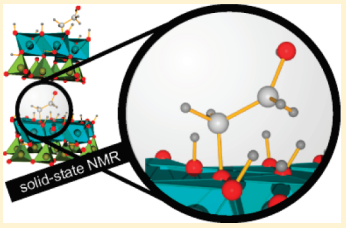

KEYWORDS: ethylene glycol intercalated kaolinite, solid-state NMR, covalent grafting, nanocomposites, surface modification, MQMAS, REAPDOR

1. INTRODUCTION

For the last decades, polymer-matrix-based nanocomposites have become a very popular scientific field of research in the area of nanotechnology.[1] Clay-based nanocomposites are of special interest owing to the large aspect ratios of clay platelets.[2,3] The resulting nanocomposites feature improved material properties compared to the pristine polymer. These enhanced properties are multifaceted and range from flame retardance[4,5] and gas barrier[6,7] to an increase of the mechanical stability, e.g., an increase of Young's modulus.[8]

A major problem in the field of inorganic particle-based polymer nanocomposites is the weak interaction between the inorganic filler and the polymer matrix, which is a consequence of the incompatibility of both materials at the interface.[9,10] Hence, an appropriate modification of the filler must be achieved in order to optimize the interaction at the interface. For fillers carrying a surface charge, a convenient and well-established way to improve the mismatch in the surface tension is ion exchange with polyelectrolytes. Such a surface modification through Coulomb interactions is the method of choice, for instance, for 2:1 layered silicates like hectorite, where both basal planes of the platelets carry a permanent negative charge.[11] However, covalent grafting to neutral functional surface groups is more challenging. μ-Hydroxyl groups are frequently encountered capping groups on external surfaces of various minerals that are often used as fillers in composite materials. Covalent grafting to this functional group would therefore offer a versatile and attractive approach to surface modification. The surface modification of such materials could, for example, be realized by covalent grafting by etherification using diols.[12] This reaction with diols has been proposed for surfaces of a range of compounds, like zirconium phosphate,[13] lepidocrocite,[14] gibbsite,[15] boehmite,[16] and kaolinite.[12] However, all of these studies have struggled with the sensitivity and surface specificity of the analytics. Until now, all evidence for covalent grafting has been solely based on IR and thermogravimetric analysis (TGA) data, which only provide indirect evidence. Therefore, we seek a direct measurement delivering unequivocal proof of such a covalent bond.

A well-suited method to prove the existence of covalent grafting on the atomic scale is solid-state NMR. Unfortunately, covalent bonding of any potential modificator will be restricted to monolayer coverage of the accessible surfaces. Consequently,

Received: January 24, 2011
Revised: April 28, 2011
Published: June 08, 2011

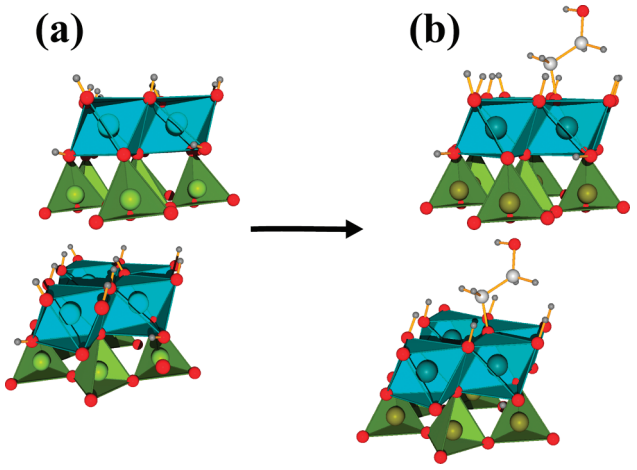

Figure 1. Structures of (a) kaolinite consisting of blue edge-sharing $Al_2(OH)_4$ octahedra and green corner-sharing SiO_4 tetrahedra and (b) EG-intercalated kaolinite.

a very large specific surface area is a prerequisite to push the sensitivity for these surface species above the detection limit. However, even for nanoscopic particles, the surface/volume ratio is still comparatively low. Thus, all bulk methods, like NMR, will struggle to detect surface species. In that respect, intercalation compounds, wherein all basal planes are exposed to potentially reactive intercalated guest molecules,[11] are ideally suited for studying the feasibility of surface modification by covalent grafting. The huge (internal) specific surface area (over 1000 $m^2\ g^{-1}$) vastly improves the sensitivity.

The 1:1 dioctahedral layered mineral kaolinite $Al_2Si_2O_5(OH)_4$ is one of the most ubiquitous clays on earth. One side of each kaolinite lamella consists of an $Al_2(OH)_4$ octahedral sheet that is capped by μ-hydroxyl groups, while the other side is composed of oxygen atoms of the SiO_4 tetrahedral sheets.[17−19] The kaolinite lamellae are stacked in a polar mode by strong hydrogen bonds (Figure 1a), forming platy crystals approximately 100 nm thick. Consequently, the outer basal surface of the clay platelet is extremely small compared to the inner surface. Fortunately, kaolinite offers a rich intercalation chemistry, and many polar neutral guest molecules as well as larger organic moieties may be incorporated into the interlamellar space.[20−26]

In the case of ethylene glycol intercalated kaolinite (EG kaolinite; Figure 1b), it has long been proposed that, beyond a purely physical incorporation of EG into the interlamellar space, reaction of the EG molecules and the μ-hydroxyl groups of the octahedral layer might take place.[12] In 1993, Tunney and Detellier[12] proposed for the first time a covalent bond of the intercalated EG molecules and kaolinite (Figure 1b). Pieces of evidence presented in that work for covalent Al−O−C bonds were an increased thermal stability/delayed deintercalation, an extended stability of the intercalated species against different solvents as well as changes in the IR spectrum.[27] The IR spectrum features a specific C−O−Al band and exhibits variation of the internal OH bands of kaolinite. Unfortunately, the specific C−O−Al band is superimposed on a band of pristine kaolinite itself,[28] weakening this piece of evidence. Moreover, it is known that the internal OH bands of kaolinite are shifted not only by grafted molecules but also by physical intercalation of molecules that simply form hydrogen bonds with kaolinite.[29−31] Although all experimental data are consistent with a covalent bond, unequivocal proof is still lacking. Moreover, quantifying the fraction of OH groups that effectively reacted to Al−O−C bonds and identifying a technique that structurally characterizes the products of the grafting reaction are desirable.

2. EXPERIMENTAL DETAILS

2.1. Materials. Well-crystallized kaolinite was obtained from Gebrüder Dorfner GmbH & Co. Kaolin- and Kristallquarzsand-Werke KG (Hirschau, Germany). Kaolinite was further purified by the removal of calcium and magnesium carbonates with ethylenediaminetetraacetic acid,[32] followed by deferration via the dithionite−citrate−bicarbonate method,[33] and by ozonization. The particle size of the material was fractionated to <5 μm by the Atterberg procedure.[34] This material was used in all of our experiments. The purity of kaolinite was confirmed by applying powder X-ray diffraction (PXRD), solid-state nuclear magnetic resonance (NMR) spectroscopy, IR spectroscopy, energy-dispersive X-ray spectroscopy, and mass spectrometry coupled to thermogravimetry (TG−MS) (not shown).

EG with a purity of 99.5% and ^{13}C-enriched EG (99 atom % ^{13}C) were purchased from Sigma Aldrich (Steinheim, Germany) and used without any further purification. Analytical-grade dimethyl sulfoxide (DMSO) was purchased by Fischer Scientific (Schwerte, Germany).

2.2. Synthesis and Analysis. The synthesis of EG kaolinite was accomplished by the guest-displacement method following literature procedures. The intermediate material, DMSO-intercalated kaolinite (DMSO kaolinite), was prepared by suspending 5 g of kaolinite in 50 mL of DMSO at a temperature of 80 °C for 7 days.[35,36] The sample was centrifuged and washed five times with 50 mL of dioxane to remove excess DMSO. DMSO kaolinite was then dried at 60 °C for 2 h and subsequently analyzed by IR, PXRD, TG-MS, and solid-state NMR (not shown). On the basis of the peak areas of the 001 reflections, the product is comprised of 98% DMSO kaolinite (d_{001} = 11.2 Å) with 2% unexpanded pristine kaolinite (d_{001} = 7.2 Å) remaining.[37]

A total of 250 mg of DMSO kaolinite was suspended in 5 mL of EG, and another 250 mg of DMSO kaolinite was mixed with 0.90 mL of ^{13}C-enriched EG in Schlenk tubes under an argon atmosphere. Both suspensions were then heated at 250 °C for 16 h.[12,30,27] The obtained EG kaolinite samples were centrifuged and washed five times with 50 mL of water and five times with 50 mL of dioxane. Finally, EG kaolinite was dried at 120 °C and analyzed by IR, PXRD, TG-MS, and solid-state ^{1}H and ^{13}C NMR (not shown). On the basis of the peak areas of the 001 reflections, the product is comprised of 97% EG kaolinite (d_{001} = 9.4 Å) with a small impurity of unexpanded kaolinite (d_{001} = 7.2 Å) remaining. All data are in perfect agreement with the 9.4 Å intercalate of Tunney and Detellier.[38]

2.3. NMR Characterization, Simulations, and Theoretical Background. The solid-state ^{1}H, ^{13}C, and ^{27}Al NMR spectra were obtained under magic-angle-spinning (MAS) conditions with a Bruker Avance II 300 spectrometer operating at 7.05 T with resonance frequencies ν_0 of 300.130, 75.468, and 78.204 MHz, respectively. All MAS measurements were carried out using a standard double-resonance 4 mm MAS probe (Bruker). The dried kaolinite samples were held in zirconia rotors and spun at 12.5 kHz. The peak positions of ^{1}H and ^{13}C NMR are referenced with respect to tetramethylsilane, while ^{27}Al NMR was referenced to $AlCl_3$ in an acidic aqueous solution ($[Al(H_2O)_6]^{3+}$). The selective ^{27}Al measurement (ν_{nut} = 13 kHz) was accomplished using three back-to-back pulses[39] with an adjusted pulse length of 3.0 μs, a continuous 50 kHz broad-band proton decoupling, and a recycle delay of 3 s to allow accurate integration of the signals.

The signals are broadened in the one-dimensional spectra because of quadrupolar interaction of the ^{27}Al nuclei ($I = {}^5/_2$), preventing identification of signals with similar isotropic shifts δ_{iso}. Two-dimensional multiquantum MAS (MQMAS) measurements offer the opportunity to

dx.doi.org/10.1021/cm200235x |*Chem. Mater.* 2011, 23, 3152–3158

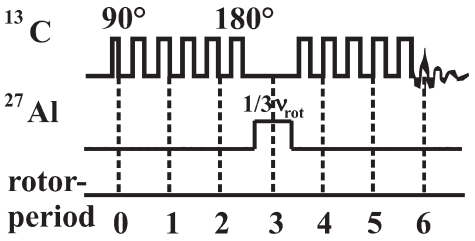

Figure 2. REAPDOR pulse sequence at six rotor periods.

overcome this problem. The quadrupolar broadening is eliminated in the F_1 dimension of a MQMAS spectrum (Figure 3a). However, quadrupolar interactions remain in the F_2 dimension, allowing for the retrieval of information about the chemical surroundings of the nuclei. Moreover, separation of the signals in the F_1 dimension may be gained by the quadrupole-induced shift of δ_{iso}.[40−42] The ^{27}Al MQMAS spectra were measured using a three-pulse sequence with nutation frequencies of 100 kHz for excitation (2.8 μs) and conversion (1.0 μs) and 13 kHz for the selective 90° pulse, respectively.[43] The coherence pathway ($0 \rightarrow \pm 3 \rightarrow 0 \rightarrow -1$) was selected via the cog-wheel phase cycle[44] COG60{11,1,0;30}, and the recycle delay was set to 1 s.

The wide-line ^{1}H and ^{13}C measurements were accomplished in a commercial double-resonance probe (Bruker) equipped with a 5 mm solenoid coil. The experiments were performed between 190 and 430 K. The solid-echo sequence was used in the case of the ^{1}H measurements with a 90° pulse length of approximately 2.05 μs. ^{13}C measurements utilized the Hahn-echo sequence with a 90° pulse length of 3.0 μs. The second moment M_2 values of the wide-line ^{1}H measurements were determined and formulated as follows (for details, see the Supporting Information):[45−47]

$$M_2 = \frac{\int \omega^2 S(\omega)\, d\omega}{\int S(\omega)\, d\omega} \quad (1)$$

The rotational echo adiabatic passage double-resonance (REAPDOR) sequence[48] has two rotor-synchronized XY-8 phase-cycled[49] 180° pulse trains on the ^{13}C channel separated by an adiabatic passage pulse on the ^{27}Al channel (Figure 2). This pulse was applied for one-third of the rotor period. To accomplish these measurements, a ^{13}C−^{27}Al overcoupled resonator was used as described in ref 50. The nutation frequency of the ^{27}Al pulse accounts for 50 kHz, while the length of the 180° pulses on the ^{13}C channel were adjusted by 6.6 μs (T = 370 K), respectively. The recycle delay was 3 s. The nutation frequency for the ^{1}H decoupling was 98 kHz during the REAPDOR sequence and 70 kHz during the acquisition.

Two sets of experiments were performed: one with (S) the adiabatic passage pulse on the ^{27}Al channel and one without (S_0) (Supporting Information, Figure S3). The number of rotor periods was stepwise increased and the difference curve ΔS normalized by S_0 (eq 2).

$$\frac{S_0(\tau) - S(\tau)}{S_0(\tau)} = \frac{\Delta S(\tau)}{S_0(\tau)} \quad (2)$$

The simulations of the REAPDOR measurements were carried out using the program *Simpson*.[51] The REAPDOR calculations were performed using a ^{27}Al−^{13}C−^{27}Al three-spin system, where the bond lengths were varied. The angles of the ^{27}Al−^{13}C dipole tensors were set as $\alpha_{1,2} = 0°$, $\beta_1 = 30°$, $\beta_2 = -30°$, $\gamma_1 = 90°$, and $\gamma_2 = -90°$. Moreover, a powder-average scheme containing 256 repulsion angles was applied. The number of gamma angles was to set 20.

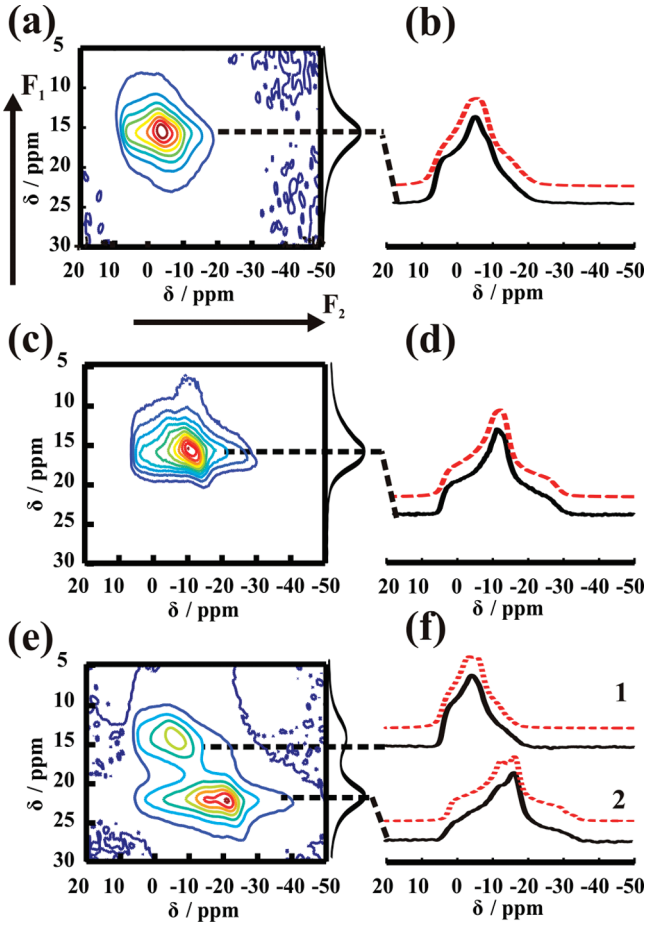

Figure 3. ^{27}Al MQMAS measurements of (a) pristine kaolinite, (c) DMSO kaolinite, and (e) EG kaolinite. (b, d, and f) Fit (dotted line) of the F_1 cross section (solid line) of kaolinite, DMSO kaolinite, and EG kaolinite spectra, respectively.

Table 1. Relevant Refined Values (Figure 3b,d,f) for the Isotropic Shift δ_{iso}, the Asymmetry Parameter η, and the QCC of the ^{27}Al MQMAS Measurements

	δ_{iso}/ppm	η	QCC/MHz
kaolinite	8.5(5)	0.70(3)	3.2(3)
DMSO kaolinite	5.8(5)	0.85(4)	3.5(2)
EG kaolinite (signal 1)	6.7(5)	0.64(2)	3.3(2)
EG kaolinite (signal 2)	3.7(5)	0.76(4)	4.4(3)

3. RESULTS AND DISCUSSION

3.1. ^{27}Al MQMAS Measurements. The ^{27}Al MQMAS measurements provide information about the local environment of the ^{27}Al nuclei within the octahedral layer, which is expected to change significantly upon covalent grafting of EG onto kaolinite.[40−42] The ^{27}Al MQMAS spectra were recorded for pristine kaolinite (Figure 3a), DMSO kaolinite (Figure 3c), and EG kaolinite (Figure 3e). Table 1 shows the values for the isotropic shift (δ_{iso}), the asymmetry parameter (η), and the quadrupolar coupling constant (QCC) as obtained by fitting the cross section in Figure 3b,d,f along the F_2 dimension by applying the program *Simpson*.[51]

dx.doi.org/10.1021/cm200235x |*Chem. Mater.* 2011, 23, 3152–3158

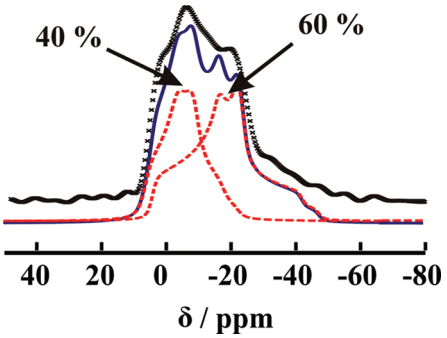

Figure 4. Fit (blue, solid line) of a selective ^{27}Al measurement (black crosses) of EG kaolinite using a spin system with two ^{27}Al species (red lines). The values for the QCC and η of the two ^{27}Al species were taken from Table 1, while δ_{iso} and the intensities were refined.

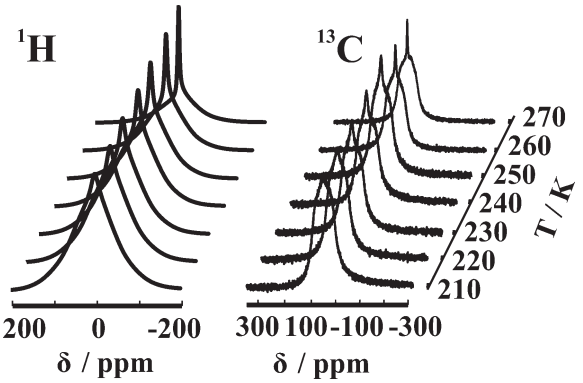

Figure 5. Normalized static solid-state ^{1}H and ^{13}C NMR measurements at temperatures between 210 and 270 K. The line-shapes of the spectra do not change much beyond 270 K.

The spectrum of pristine kaolinite reveals one signal at 8.5 ppm (Figure 3a). Consequently, every ^{27}Al nucleus in the sample has a similar chemical environment of a slightly distorted octahedron, which causes a QCC of 3.23 MHz and η of 0.7. These δ_{iso} and QCC values are in good agreement with the literature data ($\delta_{iso} = 7 \pm 1$ ppm and QCC = 3.6 ± 0.2 MHz) for pristine kaolinite.[52] This result conflicts at first glance with the kaolinite structure, which features two different crystallographic aluminum positions.[17,19] Nevertheless, these positions are apparently so similar in terms of their chemical environment that the two positions cannot be resolved by NMR. Similarly, the ^{27}Al MQMAS spectrum of DMSO kaolinite exhibits also only one signal (Figure 3c). Intercalation of DMSO into the interlamellar space causes a small change in the shape of the signal along the F_2 dimension. This is attributed to a slight increase of the QCC (Figure 3d and Table 1), which might indicate hydrogen bonding between the DMSO guest molecules and the kaolinite host.

Contrary to the data of both pristine kaolinite and DMSO kaolinite, the ^{27}Al MQMAS spectrum of EG kaolinite clearly shows two different signals (Figure 3e). These two signals represent two ^{27}Al species with notably different chemical surroundings. Signal 1 (Figure 3e,f) is similar to that of pristine kaolinite, while the other signal is shifted, indicating a significant change in the ^{27}Al chemical surroundings (Table 1) by an additional distortion of the octahedral surroundings. The aluminum species 1 is not affected by incorporation of the EG molecules in the interlamellar space, while the second species (signal 2, Figure 3f) is. Signal 2 is broader than signal 1 because of the larger QCC of 4.4 MHz, the main reason for the shift in the F_1 dimension of the spectrum. These results indicate that physical intercalation stabilized via hydrogen bonding does not significantly change the electrostatic environment of the ^{27}Al nuclei, while covalent grafting does. Consequently, the electric field gradient (EFG) turns out to be an extremely sensitive probe in this context.

Quantification of the two distinct aluminum species and, hence, the grafting density of the EG molecules within the layer is not accessible via integration of the MQMAS spectrum.[53] Therefore, a selective one-dimensional measurement was acquired. This spectrum (Figure 4, black crosses) was fitted using a spin system with two ^{27}Al species (Figure 4, dotted lines). The values for the QCC and η of the two ^{27}Al species were taken from Table 1, while δ_{iso} and the intensities were refined. The deconvolution of the two different signals yields a ratio of 40:60 for signals 1 and 2 with an error of $\pm 1\%$. Consequently, the grafting density is 0.6 EG molecules per kaolinite formula unit $Al_2Si_2O_5(OH)_4$. On the basis of the previously above-mentioned NMR experiment, we suggest the following formula for the hybrid compound: $Al_2Si_2O_5(OH)_{3.4}(OC_2H_4OH)_{0.6}$. This grafting density as determined by NMR is slightly lower than that suggested by Tunney and Detellier[38] based on TGA measurements [$Al_2Si_2O_5(OH)_{3.2}(OC_2H_4OH)_{0.8}$]. Considering that the TGA experiment is hampered by a gradual transition and partial overlap of weight losses due to desorption of EG and dehydroxylation of the kaolinite structure itself, the agreement between the two methods is surprisingly good. Please note that affirmation of the prior mentioned composition by CHN elemental analysis is tricky. In our experience, part of C/N is trapped in the material even at high temperatures and, therefore, the combustion is incomplete.[54] As might be expected considering the spatial requirements of the EG molecules, grafting of all μ-bridged aluminol groups is not feasible. The NMR experiments provide the formula $Al_2Si_2O_5(OH)_{3.4}(OC_2H_4OH)_{0.6}$ as a reasonable composition for this hybrid compound.

3.2. Distance Measurements on EG Kaolinite. Subsequently, the ^{13}C···^{27}Al distance was determined in order to unequivocally prove a direct covalent bond. This was achieved by measuring the ^{13}C···^{27}Al distance in the ^{13}C−O−^{27}Al moiety by REAPDOR measurements.[55] These measurements yield the ^{13}C···^{27}Al distance by fitting of the data with an adequate ^{13}C···^{27}Al spin system and by extraction of the heteronuclear dipolar coupling constant. Because the dipolar coupling is strongly influenced by dynamic processes, it is necessary to extract information about the temperature dependence of molecular dynamics of the EG molecules first. Only then the REAPDOR experiment can be evaluated properly.

Information on the dynamics of the hybrid system was obtained by wide-line ^{1}H NMR and wide-line ^{13}C NMR measurements at temperatures ranging between 134 and 430 K. In Figure 5, the ^{1}H and ^{13}C NMR spectra are displayed as a function of the temperature (210−270 K). The full width at half-maximum (fwhm) of the ^{1}H NMR spectra decreases with increasing temperature, while the fwhm of the ^{13}C NMR spectra does not change with the exception of a mobile impurity, a minute fraction of nonbonded excess of EG.

On the basis of these static ^{1}H measurements (Figure 5, left), the values of the second moment M_2 of the EG kaolinite system were calculated according to eq 1.[45−47] The M_2 value of the ^{1}H nuclei in the slow-motion limit is proportional to the homo- and

dx.doi.org/10.1021/cm200235x |Chem. Mater. 2011, 23, 3152–3158

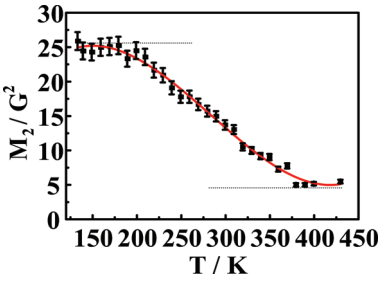

Figure 6. Second moment M_2 (black squares) for ^{1}H as a function of the temperature, calculated from static ^{1}H NMR measurements. A polynomial curve is provided as a guide for the eyes.

heteronuclear distances Σr_{ij}^{-6} of the nuclei (for details, see eqs S1 and S2 in the Supporting Information). Fast dynamical processes, however, lead to an averaging of the orientation-dependent dipole couplings, resulting in a narrowing of the absorption lines and the subsequent reduction of M_2.

Figure 6 shows the obtained M_2 values versus temperature. The error was estimated to be 5%. The curve levels off below 200 K and above 370 K, whereas in the temperature region in between, a negative slope is observed (Figure 6, red line). The activation energy was calculated based on the gradient of the slope and found to be between 3 and 8 kJ mol^{-1}, which is a quite low activation barrier for the movement of the EG molecule in the interlamellar space (for details, see the Supporting Information, Figure S2). Below 200 K, the movement of the EG molecules in the interlamellar space is slow ($\tau > 1$ ms). Therefore, the M_2 values of the protons have a constant value of 26 G^2. At 370 K, the movement of the EG molecules has become too fast for a line-shape analysis of the wide-line ^{1}H NMR spectra ($\tau < 1$ μs), resulting in a small but constant value M_2 of 6 G^2.

Further interpretation of the dynamics of EG in the interlamellar space requires a structural model. Unfortunately, intercalation compounds of kaolinite suffer from translational disorder, and such structural models cannot be extracted from XRD data. Thus, a rough model was deduced by applying computational chemistry (Figure 1). Starting with the available structure of kaolinite,[19] the interlamellar space was enlarged to meet the experimentally observed basal spacing of EG kaolinite. Next, EG molecules were grafted to the octahedral layer, for simplification with a topped-off density of 0.5 EG/formula unit. Finally, while the host structure was constrained, the configuration of EG was relaxed by applying the discover module[56] (MS Modeling 4.0 by Accelrys) and by applying the smart minimizer and the augmented *cvff_* force field.[57] The smart minimizer automatically applies different minimizing algorithms (steepest descent, conjugate gradient, and Newton method) in a cascade fashion. On the basis of this structural model of EG kaolinite, the theoretical M_2 value below 200 K was calculated by applying eqs S1 and S2 (see the Supporting Information).[58] The calculated M_2 value of 30 G^2 for the slow motion is in good agreement with the experimental value of 26 G^2, legitimizing the initial structural model derived by computational methods.

Above 370 K (dynamically disordered state), the most probable dynamical process for the EG molecules is a circular motion within the interlamellar space. Independent of the type (large angle jump or diffusion), the M_2 values can be calculated by the generation of three additional orientations by 90° rotations of the EG molecule around the c^* axis. The only degree of freedom of

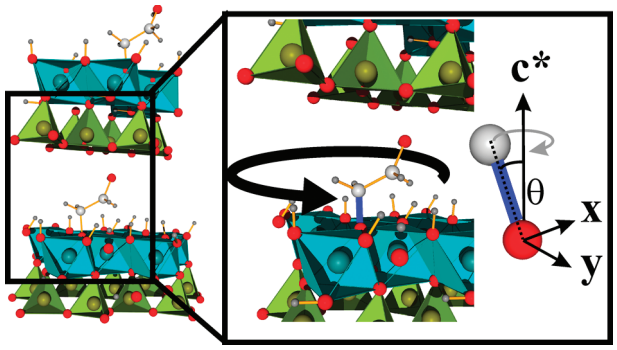

Figure 7. Dynamics of the EG molecules above 370 K and their spatial arrangement in the interlayer with a possible tilting of the EG molecules relative to c^* (Al, turquoise; O, red; C, white; H, dark gray; Si, green).

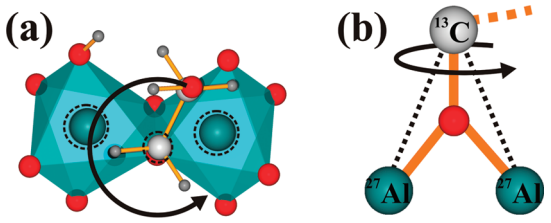

Figure 8. (a) Close-up of the bond motif in EG kaolinite (Al, turquoise; O, red; C, white; H, dark gray). The spin system is marked by black dashed circles; the black arrow clarifies the dynamic in the system. (b) Scheme of the ^{27}Al···^{13}C spin system. The orange lines stand for the covalent bonds, while the black dotted lines point out the distance measured by REAPDOR.

the EG molecule is the tilt angle θ of the C−O bond of the grafted EG molecule with respect to c^*. Applying eqs S3 and S4[58] (see the Supporting Information) on the simulated structure with a tilt angle of 10° (Figure 7) results in a value of 7 G^2. This is in perfect agreement with the experimental data of 6 G^2 and therefore indicated a circular precession or a circular jump motion of the EG molecules within the interlamellar space (Figure 7, right). Furthermore, the invariance of the ^{13}C NMR spectra as a function of the temperature (Figure 5, right) also supports a circular motion of the EG molecules around the c^* axis, as depicted in Figure 7 (for details, see the Supporting Information).

The fast circular motion of the EG molecules around the c^* axis above 370 K renders the determination of the distance between the bonded ^{13}C nuclei of EG and the ^{27}Al nuclei of the octahedral layer of kaolinite by straightforward REAPDOR measurements. Only the directly bonded ^{13}C nucleus has a unique distance to the ^{27}Al nuclei of the kaolinite layer (Figure 8a black dashed circles). The strength of the ^{13}C···^{27}Al dipole interaction for the not directly bonded CH_2OH group is small because of the circular motion and the considerably longer distances compared to the bonded ^{13}C···^{27}Al distances. Simulations, including this interaction, do not show any significant influence on the behavior of the initial REAPDOR curve ($\tau < 2$ ms). Moreover, the homonuclear dipolar ^{13}C−^{13}C interaction is averaged because the angle between of the ^{13}C−^{13}C and the crystallographic c^* axis is close to the magic angle. Please note that a detailed discussion about the choice of the three-spin system is presented in the Supporting Information. Therefore, the bonded ^{13}C nucleus and the two ^{27}Al nuclei of the kaolinite lamella build up the spin

dx.doi.org/10.1021/cm200235x |*Chem. Mater.* 2011, 23, 3152–3158

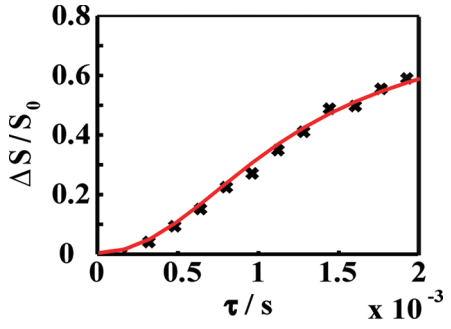

Figure 9. REAPDOR measurement at 370 K (ν_{rot} = 12.5 kHz; XY-8[49]) and simulation with the program *Simpson*[51] (red line). The error of the REAPDOR measurement is small, increasing from ±0.0006 ($\Delta S/S_0$) at the beginning to ±0.02 ($\Delta S/S_0$) at 2 ms. Because the size of the crosses is already in the range of error, the error bars are not shown.

system for simulation of the achieved $^{13}C\cdots^{27}Al$ REAPDOR measurement at 370 K (Figure 8b).

The dephasing of the ^{13}C signal under the influence of the $^{13}C\cdots^{27}Al$ dipole interaction is shown in Figure 9 at 370 K (black crosses), and selected original data are presented in Figure S3 (Supporting Information). For comparison, the measurement was also performed at room temperature (see the Supporting Information, Figure S4).

Simulations of the data were accomplished with the three-spin system depicted (Figure 8) and two equal $^{13}C\cdots^{27}Al$ distances. The number of parameters was reduced by extracting the Euler angles β_1 and β_2 of the two dipole tensors between the ^{13}C and ^{27}Al from the structure shown in Figure 7. The opening angle between the two dipole tensors is approximately 60°, and therefore β_1 is accepted to be 30° and β_2 to be −30°. Moreover, because of η being zero, the Euler angle α results in α = 0°. Furthermore, the Euler angles γ_1 and γ_2 of the dipole tensors have to be derived according to the structure and refined iteratively. γ_1 and γ_2 were determined to be 90° and −90°, respectively. Simulation using a dipolar coupling constant of 240 Hz (Figure 9, solid line) was in excellent agreement with the measurement. A coupling constant of 240 Hz results in a $^{13}C\cdots^{27}Al$ distance of 3.2 Å. The consideration of a weaker $^{13}C\cdots^{27}Al$ dipolar coupling results in an uncertainty of 10% for the $\Delta S/S_0$ values. Consequently, the error of the bond length is about 0.1 Å.

As was previously mentioned, the C−O bond between the rotating EG and the kaolinite lamellae is not parallel to c^* but slightly tilted (Figure 7, right). Consequently, the ^{13}C nucleus precesses on a cone, and the dipole coupling between the ^{27}Al nuclei and the ^{13}C nucleus is reduced. Therefore, the calculated distances tend to be overestimated compared to reality. The value of 3.2 Å can thus be understood as the upper limit for the distance between the ^{13}C of the bonded EG and the ^{27}Al of the kaolinite lamella. On the basis of the tilt angle θ of 10°, as determined from the ^{1}H line-shape analysis, the distance is reduced to 3.1 Å.

Using literature values[17,59] of 1.9 Å for the Al−O bond and 1.43 Å for the O−C bond, respectively, and a bond angle of 124° (Al−O−C), the $^{13}C\cdots^{27}Al$ distance for covalently grafted EG is expected to be approximately 3 Å. Hence, the experimental distance of 3.1 Å is in very good agreement with this estimated $^{13}C\cdots^{27}Al$ distance. For comparison, typical nonbonding Al−C distances, as determined by single-crystal structure refinement for an organometallic complex ($(^tBu)_3Al[OC(OPh)_2]$) with a similar Al−O−C geometry[60] as in the proposed EG kaolinite system, are 2.9 Å.

The distance for covalently grafted EG is significantly shorter than those found in ordinary "physical intercalates". For instance, in DMSO kaolinite the shortest distance between the ^{13}C nuclei of DMSO and the ^{27}Al nuclei of kaolinite is reported to be larger than 4.2 Å.[35] This comparison underlines that a distance of 3.1 Å between the ^{13}C nucleus of the EG molecule and the ^{27}Al nuclei of kaolinite can only be realized by a covalent bond.

4. CONCLUSION

All NMR data presented in this paper clearly show that kaolinite is grafted covalently by EG. The ^{27}Al MQMAS measurements demonstrated that the chemical environment of 60% of the ^{27}Al atoms in the octahedra differ significantly from pristine kaolinite and other ordinary intercalates like DMSO kaolinite. At temperatures above 370 K, the EG molecules precess quickly in the interlamellar space. The C−O bond of the EG molecule is tilted by 10° with respect to the c^* axis. Moreover, the distance between the bonded ^{13}C nucleus of the EG molecule and the ^{27}Al nuclei of the kaolinite layer was determined by REAPDOR measurements to be 3.1 Å.

However, the relevance of this result extends far beyond the actual implications for the model compound kaolinite itself. If μ-aluminol groups may be covalently grafted by etherification using diols, it would be expected that μ-hydroxyl groups are reactive enough to allow surface modification in general. Because μ-hydroxyl groups are frequently encountered capping groups on external surfaces of various minerals including all aluminum oxides and hydroxides as well as iron oxides and hydroxides (e.g., lepidocrocite), covalent grafting to this functional group would therefore offer a versatile and attractive approach to surface modification of all of these materials when used as fillers in composite materials.

■ ASSOCIATED CONTENT

Supporting Information. Detailed information about calculation of the M_2 values as well as the Arrhenius plot and details concerning the *Simpson* calculations. This material is available free of charge via the Internet at http://pubs.acs.org.

■ AUTHOR INFORMATION

Corresponding Author

*E-mail: juergen.senker@uni-bayreuth.de (J.S.), josef.breu@uni-bayreuth.de (J.B.). Fax: (+49) 921-552788. Telephone: (+49) 921-552531.

■ ACKNOWLEDGMENT

We thank the Deutsche Forschungsgemeinschaft (SFB 840), the Elite Study Program "Macromolecular Science", as well as the International Graduate School "Structure, Reactivity and Properties of Oxide Materials" within the Elite Network Bavaria for financial support. The authors thank Kilian Bärwinkel and Johannes Wittmann for help with a Gaussian simulation. Moreover, the authors gratefully acknowledge Dr. Andrea Michalkova for providing atomic distances of the DMSO-intercalated kaolinite.

REFERENCES

(1) Paul, D. R.; Robeson, L. M. *Polymer* **2008**, *49*, 3187–3204.
(2) Hussain, F.; Hojjati, M.; Okamoto, M.; Gorga, R. E. *J. Compos. Mater.* **2006**, *40*, 1511–1575.
(3) Manias, E.; Touny, A.; Wu, L.; Strawhecker, K.; Lu, B.; Chung, T. C. *Chem. Mater.* **2001**, *13*, 3516–3523.
(4) Berta, M.; Saiani, A.; Lindsay, C.; Gunaratne, R. *J. Appl. Polym. Sci.* **2009**, *112*, 2847–2853.
(5) Morgan, A. B. *Polym. Adv. Technol.* **2006**, *17*, 206–217.
(6) Choudalakis, G.; Gotsis, A. D. *Eur. Polym. J.* **2009**, *45*, 967–984.
(7) Maiti, P.; Yamada, K.; Okamoto, M.; Ueda, K.; Okamoto, K. *Chem. Mater.* **2002**, *14*, 4654–4661.
(8) Kunz, D. A.; Max, E.; Weinkamer, R.; Lunkenbein, T.; Breu, J.; Fery, A. *Small* **2009**, *5*, 1816–1820.
(9) Reichert, P.; Nitz, H.; Klinke, S.; Brandsch, R.; Thomann, R.; Mulhaupt, R. *Macromol. Mater. Eng.* **2000**, *275*, 8–17.
(10) Mulhaupt, R.; Stricker, F. *Kunst. -Plast. Eur.* **1997**, *87*, 482–495.
(11) Lagaly, G.; Beneke, K. *Colloid Polym. Sci.* **1991**, *269*, 1198–1211.
(12) Tunney, J. J.; Detellier, C. *Chem. Mater.* **1993**, *5*, 747–748.
(13) Yamanaka, S.; Sakamoto, K.; Hattori, M. *J. Phys. Chem.* **1984**, *88*, 2067–2070.
(14) Kikkawa, S.; Kanamaru, F.; Koizumi, M. *Inorg. Chem.* **1976**, *15*, 2195–2197.
(15) Inoue, M.; Tanino, H.; Kondo, Y.; Inui, T. *Clays Clay Miner.* **1991**, *39*, 151–157.
(16) Masashi, I. *Inorg. Chem.* **1987**, *27*, 215–221.
(17) Bish, D. L.; Vondreele, R. B. *Clays Clay Miner.* **1989**, *37*, 289–296.
(18) Kogure, T.; Elzea-Kogel, J.; Johnston, C. T.; Bish, D. L. *Clays Clay Miner.* **2010**, *58*, 62–71.
(19) Neder, R. B.; Burghammer, M.; Grasl, T.; Schulz, H.; Bram, A.; Fiedler, S. *Clays Clay Miner.* **1999**, *47*, 487–494.
(20) Duer, M. J.; Rocha, J.; Klinowski, J. *J. Am. Chem. Soc.* **1992**, *114*, 6867–6874.
(21) Li, Y. F.; Sun, D. W.; Pan, X. B.; Zhang, B. *Clays Clay Miner.* **2009**, *57*, 779–786.
(22) Komori, Y.; Sugahara, Y.; Kuroda, K. *J. Mater. Res.* **1998**, *13*, 930–934.
(23) Komori, Y.; Enoto, H.; Takenawa, R.; Hayashi, S.; Sugahara, Y.; Kuroda, K. *Langmuir* **2000**, *16*, 5506–5508.
(24) Franco, F.; Cruz, M. D. R. *Clay Miner.* **2004**, *39*, 193–205.
(25) Letaief, S.; Detellier, C. *Clays Clay Miner.* **2009**, *57*, 638–648.
(26) Tonle, I. K.; Letaief, S.; Ngameni, E.; Detellier, C. *J. Mater. Chem.* **2009**, *19*, 5996–6003.
(27) Letaief, S.; Detellier, C. *Chem. Commun.* **2007**, 2613–2615.
(28) Madejova, J.; Keckes, J.; Paalkova, H.; Komadel, P. *Clay Miner.* **2002**, *37*, 377–388.
(29) Elbokl, T. A.; Detellier, C. *J. Colloid Interface Sci.* **2008**, *323*, 338–348.
(30) Janek, M.; Emmerich, K.; Heissler, S.; Nuesch, R. *Chem. Mater.* **2007**, *19*, 684–693.
(31) Letaief, S.; Elbokl, T. A.; Detellier, C. *J. Colloid Interface Sci.* **2006**, *302*, 254–258.
(32) Tucker, B.; Kurtz, L. *Proc. Soil Sci. Am.* **1961**, *25*, 27–29.
(33) Mehra, O. P.; Jackson, M. L. *Clays Clay Miner.* **1989**, *7*, 317–327.
(34) Gericke, S. *Fortschr. Landwirtsch.* **1927**, *2*, 455–457.
(35) Michalkova, A.; Tunega, D. *J. Phys. Chem. C* **2007**, *111*, 11259–11266.
(36) Thompson, J. G.; Cuff, C. *Clays Clay Miner.* **1985**, *33*, 490–500.
(37) Lim, C. H.; Jackson, M. L.; Higashi, T. *Soil Sci. Soc. Am. J.* **1981**, *45*, 433–436.
(38) Tunney, J. J.; Detellier, C. *Clays Clay Miner.* **1994**, *42*, 552–560.
(39) Zhang, S.; Wu, X. L.; Mehring, M. *Chem. Phys. Lett.* **1990**, *173*, 481–484.
(40) Kanellopoulos, J.; Freude, D.; Kentgens, A. *Solid State Nucl. Magn. Reson.* **2007**, *32*, 99–108.
(41) Fernandez, C.; Amoureux, J. P.; Chezeau, J. M.; Delmotte, L.; Kessler, H. *Microporous Mater.* **1996**, *6*, 331–340.
(42) Rocha, J.; Morais, C. M.; Fernandez, C. *Clay Miner.* **2003**, *38*, 259–278.
(43) Amoureux, J. P.; Fernandez, C.; Steuernagel, S. *J. Magn. Reson., Ser. A* **1996**, *123*, 116–118.
(44) Jerschow, A.; Kumar, R. *J. Magn. Reson.* **2003**, *160*, 59–64.
(45) Goc, R. *J. Phys.: Condens. Matter* **1999**, *11*, 2977–2982.
(46) Goc, R. *Z. Naturforsch. A* **2002**, *57*, 29–35.
(47) Vanvleck, J. H. *Phys. Rev.* **1948**, *74*, 1168–1183.
(48) Gullion, T.; Schaefer, J. *J. Magn. Reson.* **1989**, *81*, 196–200.
(49) Gullion, T.; Baker, D. B.; Conradi, M. S. *J. Magn. Reson.* **1990**, *89*, 479–484.
(50) van Wullen, L.; Kalwei, M. *J. Magn. Reson.* **1999**, *139*, 250–257.
(51) Bak, M.; Rasmussen, J. T.; Nielsen, N. C. *J. Magn. Reson.* **2000**, *147*, 296–330.
(52) Ashbrook, S. E.; McManus, J.; MacKenzie, K. J. D.; Wimperis, S. *J. Phys. Chem. B* **2000**, *104*, 6408–6416.
(53) Amoureux, J. P.; Fernandez, C.; Frydman, L. *Chem. Phys. Lett.* **1996**, *259*, 347–355.
(54) Stocker, M.; Seyfarth, L.; Hirsemann, D.; Senker, J.; Breu, J. *Appl. Clay Sci.* **2010**, *48*, 146–153.
(55) Gullion, T. *Chem. Phys. Lett.* **1995**, *246*, 325–330.
(56) Allen, M. P.; Tildesley, D. J. *Computer Simulation of Liquids*; Clarendon Press: Oxford, U.K., 1987.
(57) Dauberosguthorpe, P.; Roberts, V. A.; Osguthorpe, D. J.; Wolff, J.; Genest, M.; Hagler, A. T. *Proteins* **1988**, *4*, 31–47.
(58) Reynhardt, E. C. *J. Phys. C: Solid State Phys.* **1986**, *19*, 1823–1836.
(59) Pauling, L. *J. Am. Chem. Soc.* **1947**, *69*, 542–553.
(60) Branch, C. S.; van Poppel, L. G.; Bott, S. G.; Barron, A. R. *J. Chem. Crystallogr.* **1999**, *29*, 993–996.